BBA - Molecular Basis of Disease 1871 (2025) 167946

Contents lists available at ScienceDirect

BBA - Molecular Basis of Disease

journal homepage: www.elsevier.com/locate/bbadis

Regular Paper

Calreticulin (*crt-1*) silencing reduces Aß$_{1–42}$-induced toxicity and restores muscle function in *C. elegans*.

Elena Caldero-Escudero, Silvia Romero-Sanz, Pilar Álvarez-Illera, Sergio De la Fuente, Paloma García-Casas, Rosalba I. Fonteriz, Mayte Montero, Javier Álvarez, Jaime Santo-Domingo *

Departamento de Bioquímica y Biología Molecular y Fisiología, Facultad de Medicina, Unidad de Excelencia Instituto de Biomedicina y Genética Molecular (IBGM), Universidad de Valladolid y Consejo Superior de Investigaciones Científicas (CSIC), Ramón y Cajal, 7, E-47005 Valladolid, Spain

ARTICLE INFO

Keywords:
C. elegans
Calreticulin
Crt-1
Alzheimer's disease
beta-amyloid
Mitochondria
Ca^{2+} signaling

ABSTRACT

Accumulation of aggregated β-amyloid peptide is a key histopathological feature of Alzheimer's Disease (AD). Experimental models of AD based on β-amyloid peptide display calcium (Ca^{2+}) signaling alterations, and targeting key components of the cellular Ca^{2+} signaling system has been postulated to modulate AD onset and progression. Here we have taken advantage of a *C. elegans* strain that over-expresses the most toxic human ß-amyloid peptide (Aß$_{1–42}$) in body-wall muscle cells, to study the impact of calreticulin (*crt-1*) silencing on body-wall muscle performance. *Crt-1* knockdown reduced the percentage of paralyzed worms in a dose-dependent manner and improved locomotion parameters in free-mobility assays in Aß$_{1–42}$-overexpressing worms. At the cellular level, *crt-1* silencing prevented Aß$_{1–42}$-induced exacerbated mitochondrial respiration and mitochondrial ROS production without impacting mitochondrial sarcomere organization. *Crt-1* knockdown reduced the number and size of Aß$_{1–42}$ aggregates in body-wall muscle cells and prevented the formation of Aß$_{1–42}$ oligomers. We propose that *crt-1* depletion reduces the number of Aß$_{1–42}$ aggregates, precluding Aß$_{1–42}$-induced mitochondrial toxicity and improving muscle function. We identify *C. elegans crt-1* as a gene involved in the toxicity associated with the expression of human Aß$_{1–42}$, and thus a potential new target for treatment.

1. Introduction

Alzheimer's disease (AD) is a neurodegenerative disorder characterized by the progressive deterioration of memory and cognitive functions [1]. Although genetic factors such as mutations in APP, PSEN1/PSEN2, and APOE genes increase the risk of developing the disease, the main contributing factor for developing AD is aging [2,3]. At the physio-pathological level, AD is associated with the accumulation and aggregation of misfolded ß-amyloid peptides in the form of plaques and neurofibrillary tangles of hyperphosphorylated tau protein in the brain [4]. In turn, the accumulated misfolded proteins trigger cellular toxicity leading to oxidative stress, mitochondrial dysfunction, cell death, and synaptic loss, particularly in the hippocampus and cerebral cortex, key areas for memory [5]. ß-amyloid peptide is currently considered the main molecular driver of AD and the first FDA-approved therapies for AD target the accumulation of the peptide [6,7].

Disruption of intracellular calcium (Ca^{2+}) signaling plays a key role in the physiopathology of AD. On one hand, dysregulation of Ca^{2+} homeostasis increases β-amyloid formation and TAU phosphorylation [8–10]. On the other hand, almost every gene that increases the susceptibility to AD impacts on Ca^{2+} signaling at different levels [11]. For instance, there is solid evidence that β-amyloid 1–40 and β-amyloid 1–42 form cation-selective ion channels able to transport Ca^{2+} across biological membranes [12]. Presenilin modulates the activity of endoplasmic reticulum (ER) calcium channels, SERCA pumps and might function as an ER Ca^{2+} leak channel [13–15]. Moreover, pathogenic mutations of PSEN1/2 also perturb Ca^{2+} homeostasis [16,17]. This bulk of evidence has contributed to strengthen the so-called Ca^{2+} hypothesis of AD. According to this hypothesis, targeting selective components of the Ca^{2+} signaling toolkit might be a potential therapeutic approach to

* Corresponding author.
E-mail addresses: elena.caldero@uva.es (E. Caldero-Escudero), silvia.romero.sanz@uva.es (S. Romero-Sanz), mariapilar.alvarez.illera@uva.es (P. Álvarez-Illera), sergio.delafuente@uva.es (S. De la Fuente), paloma.garcia@uva.es (P. García-Casas), rosalba.fonteriz@uva.es (R.I. Fonteriz), mmontero@uva.es (M. Montero), javier.alvarez.martin@uva.es (J. Álvarez), jaime.santo-domingo@uva.es (J. Santo-Domingo).

https://doi.org/10.1016/j.bbadis.2025.167946
Received 21 January 2025; Received in revised form 16 May 2025; Accepted 1 June 2025
Available online 3 June 2025
0925-4439/© 2025 The Authors. Published by Elsevier B.V. This is an open access article under the CC BY-NC license (http://creativecommons.org/licenses/by-nc/4.0/).

modify the natural course of AD [18].

Calreticulin (CRT-1) is an ER Ca^{2+} binding chaperone highly conserved across species [19]. As a molecular chaperone, calreticulin binds to newly synthesized glycoproteins, facilitating proper folding of proteins into their native configuration and preventing aggregation. If a protein fails to fold correctly, calreticulin can facilitate its retention in the ER, where it is ultimately directed to degradation pathways [20–22]. As a Ca^{2+} binding protein, calreticulin displays high Ca^{2+} binding capacity (20–30 mol Ca^{2+}/ mol protein), mainly through the acidic residues of the C-domain [23]. In that way, calreticulin provides the main Ca^{2+} buffering system within the ER lumen. It is estimated that half of the Ca^{2+} stored in the ER is bound to calreticulin [21]. Moreover, calreticulin influences the activity of inositol (1,4,5)-trisphosphate ($InsP_3$) receptors, store operated Ca^{2+} channels and the sarcoplasmic/endoplasmic reticulum Ca^{2+}-ATPase (SERCA2), thereby modulating Ca^{2+} homeostasis and signaling [24–26]. This dual role in maintaining proteostasis and regulating Ca^{2+} signaling highlights the importance of calreticulin in maintaining cellular homeostasis, especially under stress conditions that may otherwise lead to protein misfolding and cellular dysfunction, and it places calreticulin as a potentially significant factor in AD pathology.

The role of calreticulin in AD pathogenesis remains under discussion in mammalian systems. Consistent with a potential role of the Ca^{2+}-dependent chaperone on AD pathology, a few reports indicate that brains and blood serum from AD patients associate with reduced levels of calreticulin [27,28]. In favor of a preventive function of calreticulin in AD pathogenesis, it was shown that under stress conditions, brain cells release calreticulin into the extracellular medium. Released calreticulin activates microglia and interacts as a chaperone with ß-amyloid to prevent ß-amyloid peptide aggregation and neuronal loss [29,30]. Furthermore, full-length calreticulin has been shown to associate with the amyloid protein precursor (APP) and the γ-secretase complex to regulate the proteolytic processing of APP to decrease ß-amyloid peptide ($Aß_{1–42}$) in cell culture supernatants [31]. Supporting a permissive role of calreticulin in AD pathogenesis, it has been proposed that calreticulin might function as a receptor for the complement system factor C1q, promoting oxidative stress and neurotoxicity in AD [32].

In nematode models, previous data points out that calreticulin loss of function might be neuroprotective [33]. *crt-1* loss of function in *C. elegans* protects against mechanosensory, dopaminergic, and motor neuron loss in genetic models of neurodegeneration induced by several gain of function mutations on Ca^{2+} channels [34–36]. In addition, ROS-mediated and mitochondrial-dependent neurodegeneration of GABAergic neurons was suppressed by *crt-1* loss of function and *crt-1* silencing respectively [37,38]. Despite this evidence, the impact of calreticulin in AD models based on ß-amyloid peptide expression has never been addressed in *C. elegans*. Here we decided to explore whether reduction of the Ca^{2+} binding chaperone *crt-1* levels also ameliorates the status of a *C. elegans* model that over-expresses the most amyloidogenic human ß-amyloid peptide ($Aß_{1–42}$) in body-wall muscle cells [39]. Our results show that knock-down of the Ca^{2+}-dependent chaperone *crt-1* prevents the accumulation of ß-amyloid aggregates and partially restores body wall muscle function and the bioenergetic status, suggesting *crt-1* levels might play a significant role in AD pathology.

2. Results

2.1. Calreticulin silencing prevents temperature-induced paralysis of GMC101 worms

Accumulation of ß-amyloid peptide ($Aß_{1–42}$) in body-wall muscle cells impairs muscle function when exposed to a temperature switch, resulting in locomotion and mobility defects [39]. We used the Aβ-induced toxicity strain, GMC101, to investigate the potential protective effect of *crt-1* silencing on the mobility phenotype through paralysis assays. Our data show that upon temperature challenge, $Aß_{(1–42)}$-overexpressing nematodes became progressively paralyzed during aging (Fig. 1A). *crt-1*silencing significantly reduced the number of paralyzed worms at day 4 of adult life (Fig. 1A, B), and nearly fully reversed the ß-amyloid-induced paralysis phenotype at day 8 (Fig. 1A, C). The prevention of the paralysis phenotype was dose-dependent (Fig. 1B-C). As previously reported, N2 worms do not paralyze upon temperature challenge and *crt-1* silencing did not impact on the N2 paralysis phenotype (Fig. 1D). *crt-1* mRNA levels were significantly reduced in *crt-1* RNAi-fed N2 and GMC101 worms, confirming effective silencing regardless of the strain used (Fig. 1E, F). These results suggest that *crt-1* loss of function protects the nematodes against $Aß_{1–42}$-induced toxicity in body-wall muscle cells.

2.2. Calreticulin knock-down improves the performance of GMC101 worms in free mobility assays

To further explore the effect of *crt-1* silencing on $Aß_{(1–42)}$-induced body-wall muscle dysfunction we studied the spontaneous motion of worms in free-mobility assays. This approach allows us to quantitatively assess the distance traveled and the speed of movement of each worm, either the maximum speed, the average speed, or the speed measured in body lengths per second (BLPS) to account for differences in worm size. Our results show that $Aß_{(1–42)}$-overexpressing worms exposed to the temperature challenge significantly reduced all mobility parameters during aging compared with N2 control worms (Fig. 2A-H). Moreover, *crt-1* silencing partially restored length traveled (Fig. 2A-B), average speed (Fig. 2C-D), and BLPS (Fig. 2E-F) at day 5 of adulthood, although it did not impact on the maximum speed (Fig. 2G-H). Intriguingly, *crt-1* silencing in N2 worms also improved all mobility parameters at day 5 of adulthood, indicating that mobility improvement driven by *crt-1* knock-down does not rely on $Aβ_{(1–42)}$-overexpression (Suppl. Fig. 1). These data suggest that reduction of *crt-1* levels enhance mobility in *C. elegans* and confirm that down-regulation of *crt-1* improves muscle performance of $Aß_{(1–42)}$-overexpressing worms.

2.3. Calreticulin knock-down preserves mitochondrial function

The accumulation of ß-amyloid peptide ($Aß_{1–42}$) interferes with mitochondrial function in different organism models and tissues [40]. Indeed, Aβ accumulation associates to mitochondrial-induced oxidative stress [41]. In turn, oxidative stress has been proposed to play a key role in triggering the GMC101 paralysis phenotype [42]. To determine whether *crt-1* silencing affects mitochondrial ROS production, we measured mitochondrial superoxide levels using MitoSOX™. As shown in Fig. 3A-B, $Aβ_{(1–42)}$-overexpressing nematodes exposed to a temperature challenge produce larger amounts of superoxide ions than N2 control worms. *Crt-1* silencing in $Aß_{(1–42)}$-overexpressing worms completely reversed superoxide production to the N2 control levels at days 4 and 8 of adult life (Fig. 3A-B). *crt-1* silencing did not impact on superoxide production in N2 control worms (Fig. 3C-D). In agreement, oxygen consumption rates (OCR) were significantly increased under basal (Fig. 3E-F) and uncoupling conditions in $Aβ_{(1–42)}$-overexpressing nematodes (Fig. 3E and G), and *crt-1* silencing fully reversed the phenotype without impacting on N2 control worms. These results indicate that ß-amyloid peptide accumulation exacerbates respiratory chain activity, enhancing electron leak and superoxide production, and *crt-1* is necessary for such actions. Mitochondrial membrane potential was unaltered in β-amyloid overexpressing worms compared to the N2 control strain (Suppl.Fig. 2A); this evidence shows that neither the burst in oxygen consumption nor superoxide production are likely driven or accompanied by changes in the mitochondrial membrane potential. We noted *crt-1* silencing decreases the mitochondrial membrane potential in $Aβ_{(1–42)}$-overexpressing nematodes (Suppl. Fig. 2A), although it did not have any impact N2 control worms (Suppl. Fig. 2B).

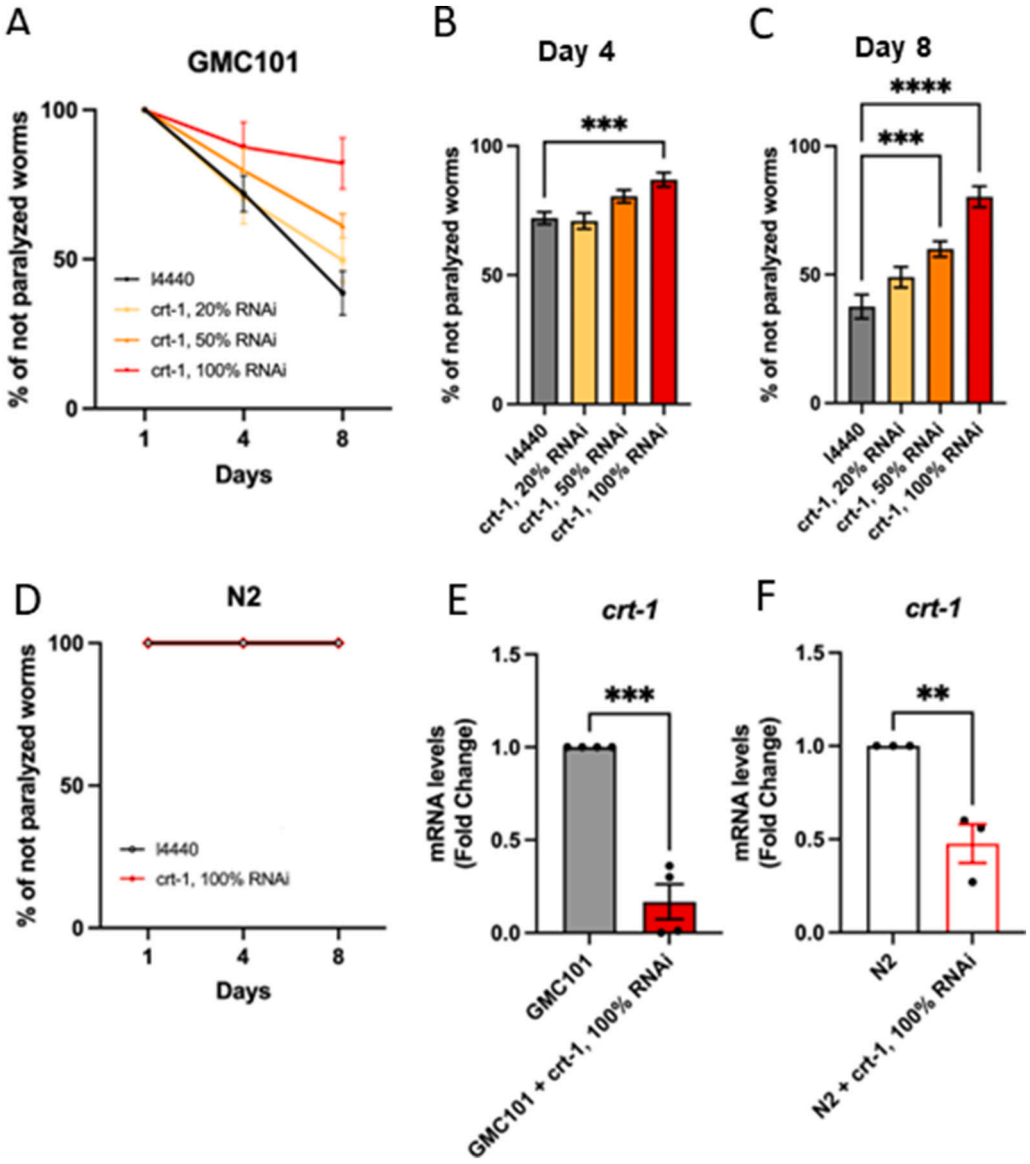

Fig. 1. Effect of calreticulin silencing on temperature-induced paralysis of GMC101 worms. A) Percentage of non-paralyzed worms fed with control bacteria (L4440), *crt-1* RNAi bacteria, or different percentages of *crt-1* RNAi / L4440 bacteria, over time. B) Percentage of non-paralyzed worms on day 4 of adulthood fed with control RNAi (L4440) or different percentages of *crt-1* RNAi / control RNAi bacteria. C) Percentage of non-paralyzed worms on day 8 of adulthood fed with control RNAi (L4440) or different percentages of *crt-1* RNAi / control RNAi bacteria. D) Percentage of non-paralyzed N2 worms over time upon *crt-1* silencing. For paralysis assays, experiments are the result of three biological replicates, each containing 3 technical replicates. E) Effect of *crt-1* RNAi on *crt-1* mRNA levels in GMC101 worms ($n = 3$, experiments). F) Effect of *crt-1* RNAi on *crt-1* mRNA levels in N2 worms on day 4 of adulthood (n = 3, experiments). Data are mean ± s.e.m. * $p < 0.05$; ** $p < 0.01$; *** $p < 0.001$; **** $p < 0.0001$.

2.4. Calreticulin silencing does not restore β-amyloid-induced sarcomeric mitochondrial disorganization in body-wall muscles

The spatial organization of mitochondrial networks in body-wall muscle cells displays a characteristic distribution, forming parallel rows of shortly elongated mitochondrial units whose spatial disposition is conditioned by sarcomeres (Fig. 4A). Loss of sarcomere and mitochondrial organization in body-wall muscle cells is associated with muscle dysfunction [43]. We visualized body-wall mitochondrial networks by using the potentiometric dye TMRE to test whether the accumulation of β-amyloid peptide in body-wall muscle cells alters mitochondrial organization and shape. As shown in Fig. 4A, β-amyloid peptide accumulation in GMC101 nematodes disorganized mitochondrial distribution. GMC101 nematodes showed a similar number of mitochondrial units per cell (Fig. 4B). Still, the area covered by mitochondria significantly decreased (Fig. 4C). Additionally, aspect ratio (Fig. 4D) and mitochondrial branch length (Fig. 4E) were significantly reduced. These results indicate that $A\beta_{1-42}$ overexpression in body-wall muscle cells triggers mitochondrial fragmentation. *Crt-1* silencing on β-amyloid overexpressing worms exhibited a tendency to restore the mitochondrial distribution on parallel rows (Fig. 4A). Although *crt-1* silencing slightly increased the number of mitochondrial units per cell, it did not restore any of the mitochondrial shaping parameters evaluated (Fig. 4B-E). We conclude that *crt-1* silencing improved the spatial disposition of mitochondria, but it does not rescue β-amyloid-induced mitochondrial fragmentation in body-wall muscles.

2.5. Calreticulin silencing reduces the number of β-amyloid aggregates in body-wall muscle cells

To explore the protective mechanisms preventing ß-amyloid-induced paralysis, we then tested whether improved muscle performance upon

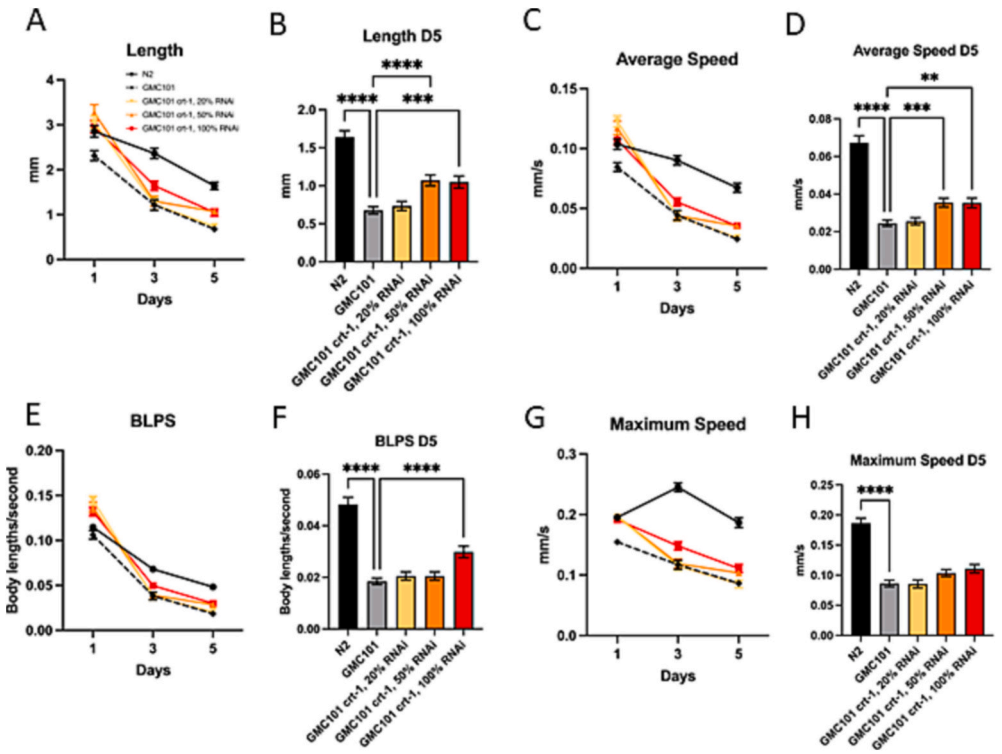

Fig. 2. Effect of calreticulin knock-down on GMC101 worms in free mobility assays. Panels A, C, E, G show mobility parameters of N2 worms and GMC101 worms fed either with control RNAi (L4440) or different percentages of *crt-1* RNAi / control RNAi bacteria, at day 1, day 3 and day 5 of adulthood. Length traveled (panel A), average speed (panel C), body lengths per second (BLPS) (panel E) and maximum speed (panel G). Panels B, D, F and H show mobility parameters of N2 and GMC101 worms fed either with control RNAi (L4440) or different percentages of *crt-1* RNAi / control RNAi bacteria, at day 5 of adulthood. Length traveled (panel B), average speed (panel D), body lengths per second (BLPS) (panel F), maximum speed (panel H). Experiments were completed with $n = 60$ animals per experimental condition. Data are mean ± s.e.m. * $p < 0.05$; ** $p < 0.01$; *** $p < 0.001$; **** $p < 0.0001$.

crt-1 silencing correlated with changes in the number and size of ß-amyloid aggregates. *In vivo* aggregates were visualized and quantified using the amyloidogenic dye Thioflavin T [39]. As expected Thioflavin T positive ß-amyloid aggregates are absent in control strain N2 (Fig. 5A-left column), which does not express any $A\beta_{(1-42)}$ mRNA (Fig. 5B). On the contrary, $A\beta_{(1-42)}$-overexpressing worms show accumulation of ß-amyloid aggregates within the head area of the body-wall muscle (Fig. 5A-midle column). *crt-1* silencing significantly reduced the number (Fig. 5A-right column and 5C) and the size of individual aggregates (Fig. 5D). Accordingly, the percentage of head area occupied by β-amyloid aggregates, calculated as the percentage of aggregates area divided by head area (slashed line), was significantly reduced (Fig. 5E). Furthermore, the fluorescence intensity of individual aggregates significantly decreased (Fig. 5F), suggesting that *crt-1* silencing also reduced the β-amyloid content of aggregates. These results cannot be attributable to reduced $A\beta_{(1-42)}$ mRNA production, as mRNA levels slightly increased upon *crt-1* silencing (Fig. 5B). Since $A\beta_{(1-42)}$ mRNA production is driven by the *myo-4* (myosin heavy chain-4) promoter, it can be hypothesized that increased body-wall muscle function upon *crt-1* silencing (Fig. 2A and Suppl.Fig. 1) may promote transcriptional activation of muscle function genes and thus $A\beta_{(1-42)}$ mRNA production, given that they share the same cis-regulatory elements. Our results suggest this may be the case, as *crt-1* silencing also promoted the transcription of the endogenous myosin heavy chain gene *myo-3* on N2 and GMC101 strains (Fig. 5G). We conclude that improved muscle performance mediated by *crt-1* silencing correlates with reduced levels of β-amyloid aggregates.

2.6. Calreticulin silencing prevents the formation of Aβ oligomers

Aβ monomers can aggregate and form larger soluble and insoluble forms. A consistent number of works reported that soluble Aβ aggregates are more neurotoxic than monomers and insoluble aggregates [44]. We therefore tested whether *crt-1* silencing in GMC101 worms modified the overall levels of β-amyloid peptide as well as the oligomerization profile. Western blotting using $A\beta_{(1-42)}$ antibodies confirmed that N2 worms do not express any $A\beta_{(1-42)}$ peptide, validating the specificity of the assay (Fig. 6A). GMC101 worms feed with control L4440 bacteria displayed a pattern of bands corresponding to the Aβ monomer at 4 kDa, Aβ dimmer at 8 kDa, Aβ trimer-tetramer around 12–16 kDa, Aβ pentamer at 20 kDa and higher molecular weight oligomers (Fig. 6A). Quantification of the full pattern of bands demonstrated that *crt-1* silencing reduced ß-amyloid levels (Fig. 6B). The intensity level of Aβ monomer and dimer bands was not significantly changed by *crt-1* silencing (Fig. 6C). On the contrary, the intensity levels of trimers-tetramers, pentamers and higher molecular weight oligomers significantly decreased upon *crt-1* silencing (Fig. 6D). These results indicate that *crt-1* silencing selectively reduces the levels of ß-amyloid oligomers in GMG101 worms. RNAi silencing of *sca-1*, the sarcoendoplasmic reticulum Ca^{2+} ATPase, a critical cellular component to maintain endoplasmic reticulum calcium homeostasis, did not modify neither the ß-amyloid levels nor the pattern of bands (Fig. 6A), suggesting that *crt-1* loss of function elicits a specific response to deplete body-wall muscle cells from ß-amyloid oligomers independent from ER Ca^{2+} levels.

3. Discussion

Loss of cellular proteostasis is a hallmark of aging and several neurodegenerative diseases including Alzheimer's disease (AD), which are pathologically characterized by the accumulation of Aβ and amyloid-like peptides [40,45]. Remodeling of Ca^{2+} signaling is intrinsically associated with AD, and AD experimental models based on Aβ

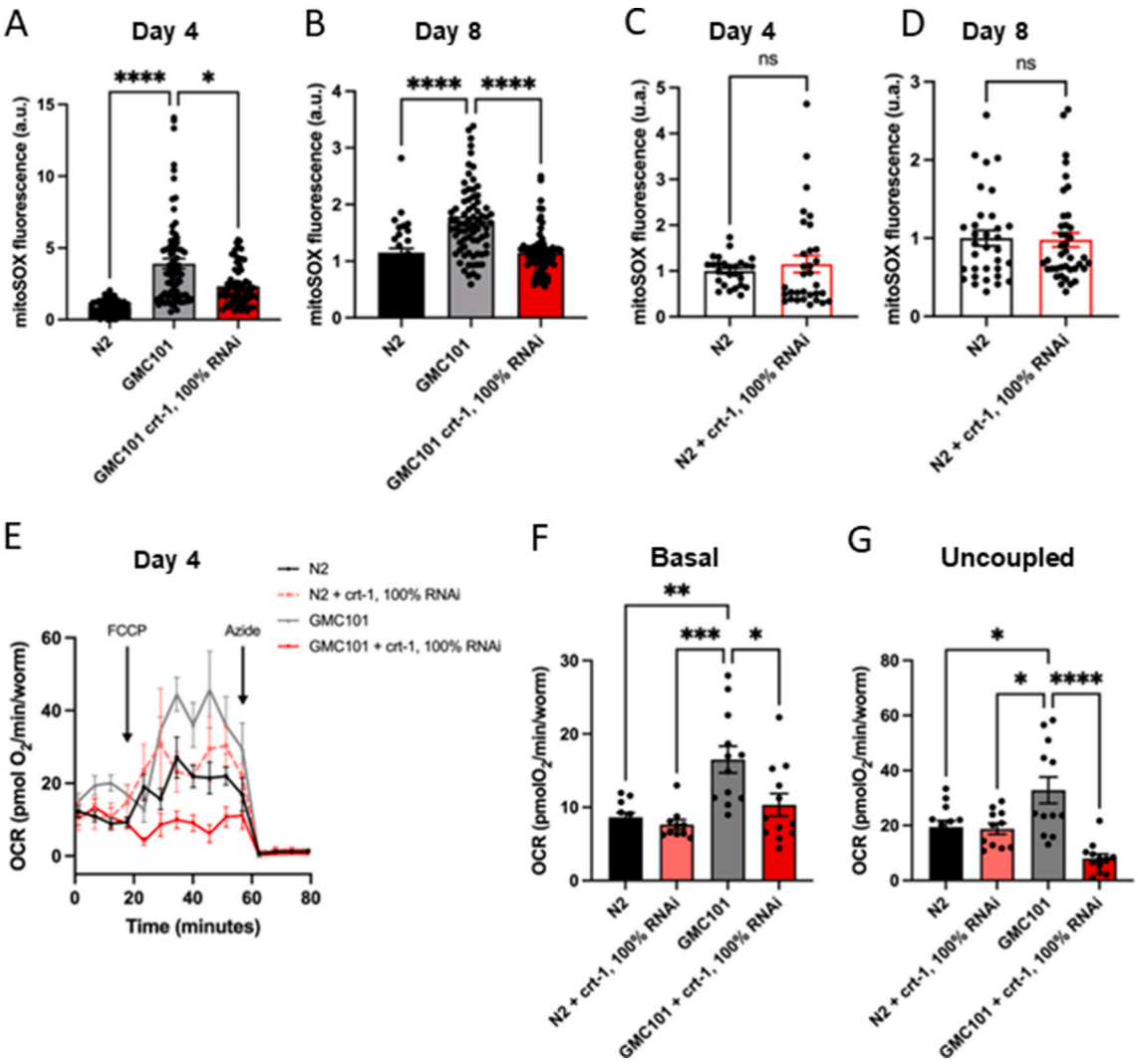

Fig. 3. Effect of calreticulin knock-down on GMC101 mitochondrial function. A) Mitochondrial superoxide production measurements with MitoSOX™ at day 4 of adulthood, and B) at day 8 of adulthood. Experiments were completed with $n = 50–80$ animals per experimental condition. C) Effect of *crt-1* silencing on mitochondrial superoxide production in N2 worms at day 4 of adulthood, and D) at day 8 of adulthood. E) Oxygen consumption rates (OCR) measurements, the protonophore FCCP, and the cytochrome C oxidase inhibitor azide, were added when indicated to obtain the maximum uncoupled respiration rate and non-mitochondrial respiration, respectively. F) Effect of *crt-1* silencing on basal respiration. G) Effect of *crt-1* silencing on maximal (uncoupled) respiration in the presence of FCCP. The data shown is the result of 4 biological replicates, each containing 4 technical replicates. Data are mean ± s.e.m. * $p < 0.05$; ** $p < 0.01$; *** $p < 0.001$; **** $p < 0.0001$.

expression display alterations in cellular Ca^{2+} homeostasis [11]. Therefore, it has been postulated that activity perturbation of different components of the Ca^{2+} signaling system may modify the natural course of the disease [18]. Our team has previously described that pharmacological and genetic inhibition of the ER Ca^{2+} ATPase *sca-1* promotes longevity in N2 *C. elegans* worms [46,47], and we have recently reported that *sca-1* silencing partially reverted the phenotype of a complex-I deficiency *C. elegans* model of Parkinson's disease (PD) [48]. These pieces of evidence point to an important role of ER Ca^{2+} in the mechanisms underlying aging and neurodegeneration in experimental models of *C. elegans*. Our new findings indicate that knockdown of *crt-1*, the main ER Ca^{2+}-buffering protein [21], partially prevents Aβ-induced toxicity in *C. elegans* body-wall muscle by reducing the formation of Aβ aggregates, pointing out that calreticulin facilitates the progression of Aß-driven pathology under physiological conditions. Moreover, in the same way that *sca-1* inhibition, *crt-1* loss of function also decreases the total Ca^{2+} stored at the ER [49]. Thus, our results contribute to support the idea that a partial reduction of ER Ca^{2+} levels is protective against different types of stress and promotes healthspan in *C. elegans*.

The nematode *C. elegans* is an excellent model to study the role of calreticulin on Aß-driven pathogenesis. The calreticulin function is highly conserved in *C. elegans*. As reported in other organisms, it contains an ER-localization C-terminal HDEL signal, shows Ca^{2+} binding properties and Ca^{2+}-dependent chaperone function, and is highly expressed in muscle cells [19], indicating that *C. elegans* is a well-defined and conserved model to study calreticulin functions. In addition, one of the main advantages of this model is that *in vivo* effects of transgenic human-Aß can be examined in isolation from endogenously produced Aß. In mammals, Aß is endogenously produced from APP by the sequential action of ß- and γ-secretases [1]. On the contrary, although *C. elegans* expresses an APP ortholog, *apl-1* (Amyloid Precursor-Like-1), it lacks ß-secretase sites and ß-secretase orthologues [39]. Therefore, *C. elegans* cannot process the Amyloid Precursor Protein (APP).

Our results show that *crt-1* silencing significantly prevented temperature-induced paralysis and improved locomotion parameters in free mobility assays of worms overexpressing Aβ on body-wall muscles (Fig. 1–2). These results suggest that downregulation of *crt-1* expression improved body-wall muscle performance impaired by Aβ accumulation.

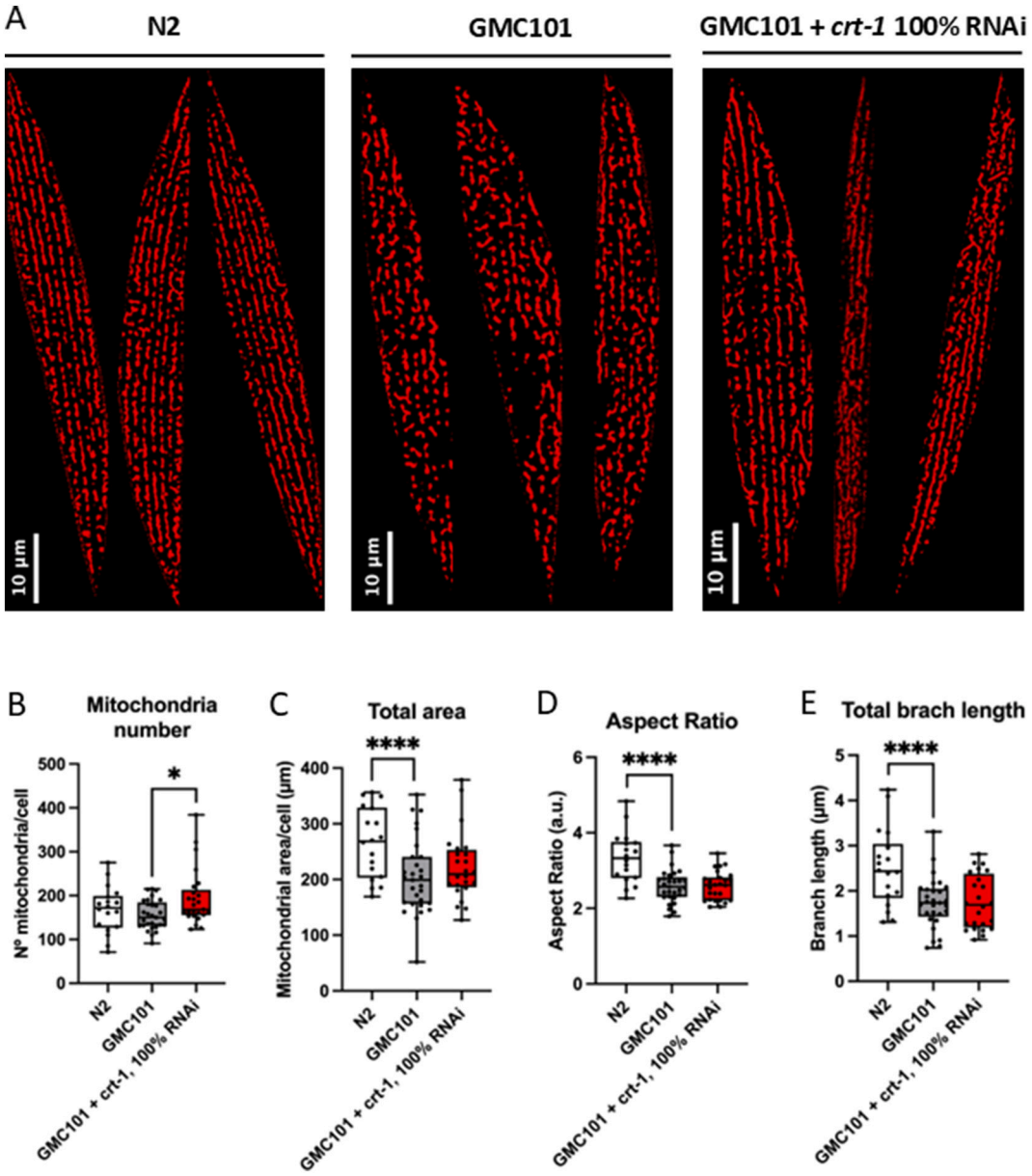

Fig. 4. Effect of calreticulin silencing on β-amyloid-induced mitochondrial disorganization in body-wall muscles. A) A series of representative confocal images of mitochondrial networks of body wall muscle cells of day 4 nematodes are shown in three different experimental conditions: N2 (control) worms, GMC101 worms (overexpressing beta-amyloid peptide), and GMC101 worms upon *crt-1* RNAi. B) Number of mitochondria per cell. C) Area covered by mitochondria per cell. D) Aspect ratio. E) Total branch length per cell. Experiments were completed with $n = 20–40$ animals per experimental condition. Group mean and variability are displayed as box plots. * $p < 0.05$; ** $p < 0.01$; *** $p < 0.001$; **** $p < 0.0001$.

The strong correlation between the percentage of *crt-1* RNAi provided and the recovery degree of the paralysis phenotype at day 8 of adulthood indicates a relationship between the levels of calreticulin and muscle performance in GMC101 worms (Fig. 1C). These results align with previous findings showing that the RNAi against *crt-1* improves the movement defect in *unc-105* gain-of-function mutants, encoding a constitutively active plasma membrane Ca^{2+} channel [50]. The protection mechanism might involve a compensatory reduction of cellular Ca^{2+} levels upon *crt-1* silencing, preventing cellular damage driven by excess of Ca^{2+} [51]. Translating this evidence to our model, it can be hypothesized that *crt-1* silencing compensates for the Aβ-induced Ca^{2+} dysregulation [11], preventing cellular damage and partially restoring body-wall muscle functionality. However, whether GMC101 worms display higher cytosolic Ca^{2+} levels in body-wall muscle cells is unknown. Our data also show that *crt-1* silencing efficiently reduced *crt-1* mRNA levels in both GMC101 and N2 worms, validating our calreticulin deficiency model. Interestingly, it has been reported that *crt-1* transcription is significantly up-regulated upon UPR activation to protect the worm from deleterious accumulation of unfolded proteins [52]. In line with this model, ER stress induced by knockdown of *crt-1*, *pdi-2* or *pdi-3* has been reported to increase the expression of *crt-1* significantly [53]. The explanation for these discrepancies remains unclear.

Aβ accumulation in AD and age-related amyloidosis are conserved factors contributing to mitochondrial dysfunction [40,45]. In our experiments, Aβ overexpression in body-wall muscle cells produced a significant increase in mitochondrial respiration (OCR), both in basal and uncoupled states (Fig. 3E-G). This increase in the electron flux of the respiratory chain complexes was consistently accompanied by a rise in mitochondrial ROS production (Fig. 3A-B), suggesting that in our model Aβ overexpression exacerbates mitochondrial respiration in an electron

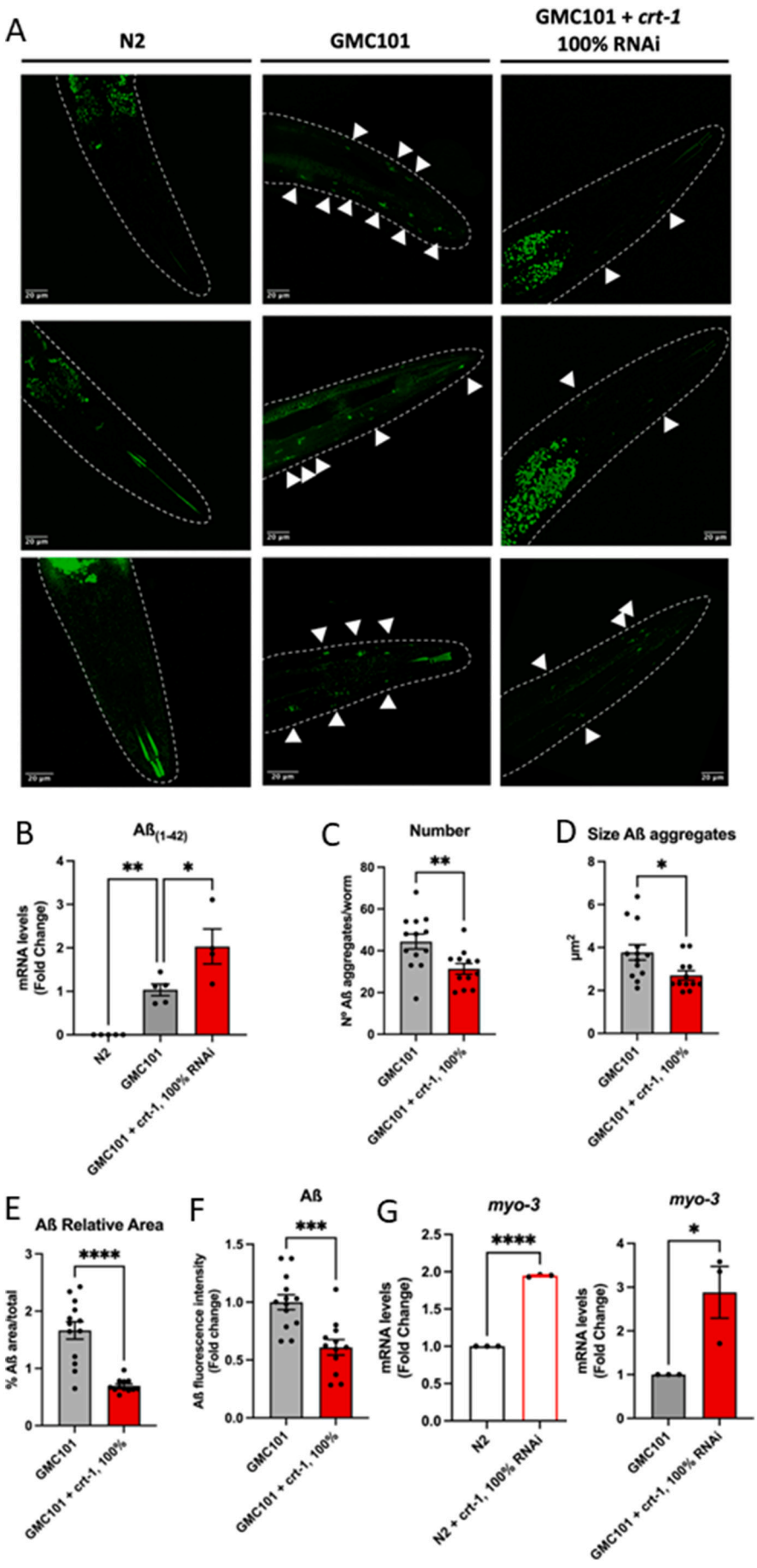

(caption on next page)

Fig. 5. Effect of calreticulin silencing on ß-amyloid aggregates. A) Representative confocal images of ß-amyloid aggregates stained with Thioflavin-T located in muscle cells at the anterior region of the body wall muscle of day 4 nematodes. B) ß-amyloid mRNA levels in N2 *versus* GMC101 worms, and effect of *crt-1* silencing on ß-amyloid mRNA levels in GMC101 worms. C) Effect of *crt-1* silencing on the number of ß-amyloid aggregates in the anterior region of the body wall muscle. D) Effect of *crt-1* silencing on the size of ß-amyloid aggregates in the anterior region of the body wall muscle. E) Effect of *crt-1* silencing on the fraction area occupied by ß-amyloid aggregates in the anterior region of the body wall muscle. F) Effect of *crt-1* silencing on the fluorescence intensity of ß-amyloid aggregates in the anterior region of the body wall muscle. Experiments were completed with $n = 10–20$ animals per experimental condition. G) Effect of *crt-1* silencing on *myo-3* mRNA levels in N2 and GMC101 worms ($n = 3$, experiments). Data are mean ± s.e.m. * $p < 0.05$; ** $p < 0.01$; *** $p < 0.001$; **** $p < 0.0001$.

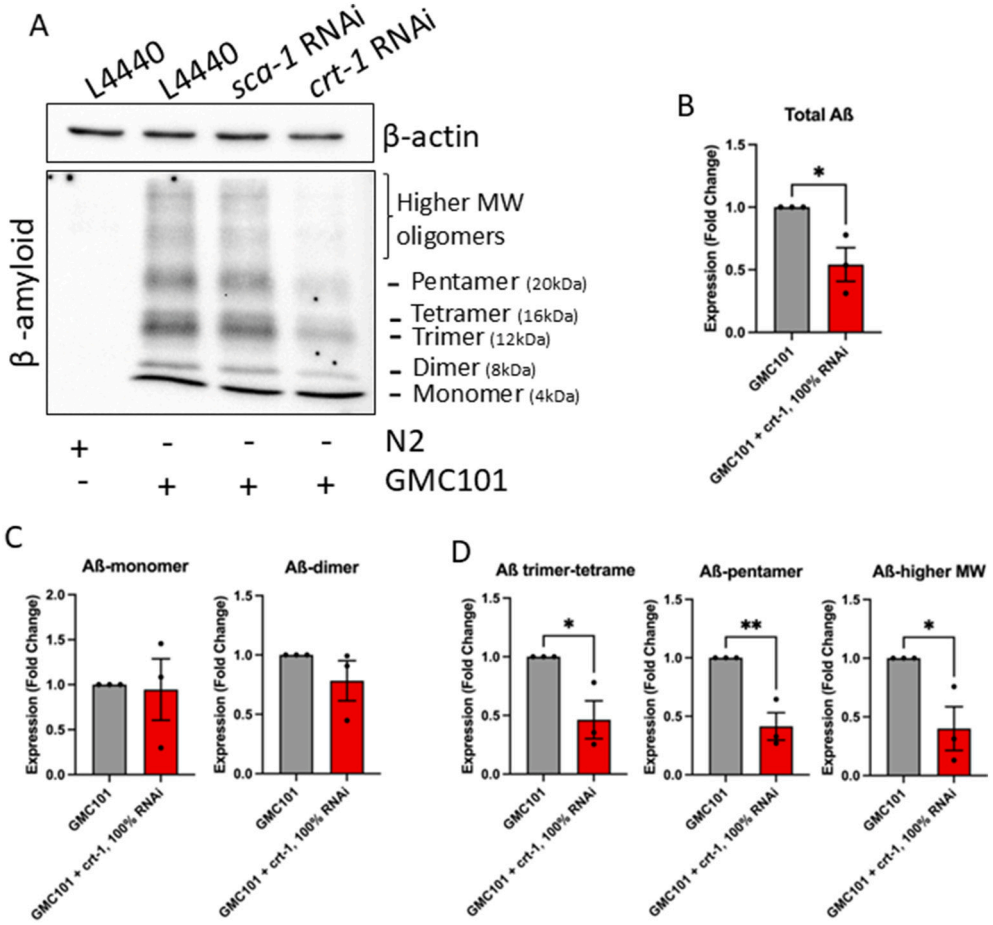

Fig. 6. Effect of calreticulin silencing on the formation of Aß oligomers. A) ß-amyloid peptide levels and aggregation in GMC101 worms upon *crt-1* RNAi shown by western blotting, a representative image of the tree biological repeats performed. B) Expression levels of total ß-amyloid peptide regardless of its aggregation degree (n = 3, experiments). C) Expression levels of ß-amyloid peptide monomers and dimers (n = 3, experiments). D) Expression levels of ß-amyloid peptide trimer-tetramer, pentamers and higher molecular weight complexes (n = 3, experiments). Data are mean ± s.e.m. * $p < 0.05$; ** $p < 0.01$; *** $p < 0.001$; **** $p < 0.0001$.

leaky mode. This functional status of the respiratory chain is not attributable to reduced mitochondrial membrane potential, as this parameter was unaffected in the GMC101 strain (Suppl.Fig. 2). Elevated ROS levels are consistent with previous reports [54] and they may significantly contribute to the body-wall muscle dysfunction phenotype of the GMC101 strain (Fig. 1–2). In addition, *crt-1* silencing restored OCR in worms overexpressing Aβ, without impacting the mitochondrial respiration of the control N2 strain, suggesting that *crt-1* knockdown specifically reverses Aβ-induced molecular events triggering the respiratory phenotype. Similar to the reduced respiration rate, ROS production returned to levels comparable to those of wild-type N2 worms upon *crt-1* silencing. Our results also show that Aβ overexpression on body-wall muscle cells disrupted mitochondrial network organization, generating a fragmented mitochondrial phenotype. This phenotype matches with previous reports [40,55]. However, although *crt-1* silencing showed a trend to rescue the fragmented mitochondrial phenotype, we could not measure significant differences in key mitochondrial morphology parameters (Fig. 4B-D). Off note, *crt-1* silencing was shown to disorganize body wall-muscle sarcomere in N2 worms [43]. We propose that the failure of *crt-1* RNAi to rescue the fragmented mitochondrial phenotype of the GMC101 strain is associated with the sarcomere structural remodeling induced by *crt-1* silencing, an event that might constrain mitochondrial distribution and shape through the sarcomere.

According to the amyloid-cascade hypothesis, Aβ accumulation is the initiating molecular event triggering neurodegeneration in sporadic Alzheimer's disease [4]. Our results indicate that *crt-1* silencing prevents accumulation of high molecular weight oligomers (Fig. 6) and Thioflavin T -visualized Aβ aggregates *in vivo* (Fig. 5). Reduced Aβ levels might therefore explain the improved body wall muscle function observed upon *crt-1* silencing (Fig. 1 and Fig. 2). In our model, Aβ levels result from a balance between transcriptional overproduction of Aβ driven by the muscle-specific promoter *unc-54/myo-4* of the pCL12 plasmid and the action of protein clearance mechanisms. We speculated that reduced Aβ levels might result from repressed transcription of Aβ trans-gene. However, we ruled out this possibility as *crt-1* silencing

significantly increased Aβ mRNA levels (Fig. 5B). This observation raises the question on why Aβ mRNA levels increase upon *crt-1* silencing. Given that GMC101 worms express Aβ under the control of the myosin-heavy chain gene-4 (myo-4) promoter, we propose that increased muscle function on *crt-1* silenced worms (Fig. 1–2) may naturally promote transcription of body-wall muscle function genes, comprising the myosin genes and other genes sharing similar promoters, including the Aβ transgene (Fig. 5G). Since *crt-1* loss of function does not reduce Aβ mRNA, it can be hypothesized that lack of *crt-1* may prevent Aβ-aggregates formation by activating protein clearance mechanisms, including ubiquitin-proteosome degradation, chaperone-mediated autophagy, or macroautophagy [56]. A plausible explanation for this phenomenon is that *crt-1* loss of function induces ER stress, resulting in compensatory activation of the chaperone *hsp-4* and UPR activation in nematodes [57]. Subsequently, UPR activation induces autophagy to clear damaged or misfolded proteins. Indeed, Aβ can be targeted for autophagy-dependent degradation within the lysosome in rodents and *C. elegans* [58,59]. Concomitantly, increased levels of cytosolic Ca^{2+} triggered by *crt-1* loss of function-dependent ER Ca^{2+} depletion may also contribute to enhancing autophagy [60]. In summary, UPR activation with the concomitant expression of chaperones and autophagy induction might lead to increased turnover of Aβ and thus contribute to eliminating Aβ aggregates to restore proteostasis.

Our findings indicate that *crt-1* expression contributes to Aβ-driven toxicity, supporting the concept that calreticulin may be an interesting exploratory therapeutic target in the context of Alzheimer's Disease. Unfortunately, modulating a cellular component widely distributed across tissues and involved in a wide range of functions, including cellular Ca^{2+} homeostasis, protein folding, and stress signaling, could lead to unintended side effects. Furthermore, its intracellular localization makes it challenging to target directly with small molecules or antibodies. Nevertheless, some of these limitations can be overcome by using viral or exosome-based RNAi delivery platforms [61]. Some attempts have been made to indirectly modulate its function or influence its cell surface presentation, but drug development is still in the early stages [62,63]. Evaluating the potential of calreticulin as a target with disease-modifying properties on Aβ-driven pathologies requires extensive additional work, including understanding the molecular mechanisms involved, experimental confirmation in rodent models, and clinical studies.

4. Material and methods

4.1. C. elegans strains and maintenance

Nematodes were maintained and handled at 20 °C on nematode growth medium (NGM) on agar plates containing *E. coli* OP50 as a food source. *C. elegans* strains N2 and GMC101 were obtained from the *C. elegans* Genetics Center (CGC, University of Minnesota, MN, USA). Strain GMC101 (dvIs100 [unc-54p::A-beta-1-42::unc-54 3'-UTR + mtl-2p::GFP]) is an N2-derived strain that produces a constitutive expression of GFP in intestinal cells and expresses full-length human $Aß_{(1–42)}$ peptide in body wall muscle cells that aggregates *in vivo* upon temperature sifting of day 1 / young adults animals from 20 to 25 °C.

4.2. RNAi interference

The HT115 RNAi clone for *crt-1* (Y38A10A.5, Ahringer library) and empty vector (L4440) were purchased from Source Biosciences (Cambridge, UK). HT115 *crt-1* RNAi and L4440 bacteria were cultured overnight at 37 °C in LB medium containing 125 μM ampicillin. Once they reached a $DO_{595} = 0.6$, *crt-1* RNAi and empty vector L4440 bacteria were mixed to the desired percentage and then 100 μl of the mixture were seeded onto 35 mm plates containing NGM agar with 1 mM isopropyl-b-d-thiogalactoside (IPTG), 50 μM carbenicillin and 15 μM fluorodeoxyuridine, and incubated for 3 days at 20 °C.

4.3. RNA isolation and quantitative real-time PCR

500–600 worms at day 3 of adulthood were collected and washed three times. Samples were subjected to three freeze/thaw cycles in liquid nitrogen. Next, the frozen samples were ground using Bel-Art® Disposable Pestles (BAF199230000) for homogenization. RNA was extracted using a phenol-chloroform method as previously described [61]. After extraction, RNA samples were incubated for 30 min at room temperature with DNase to eliminate DNA contamination (RNase-Free DNase Set, Quiagen, 79254). The integrity of the extracted RNA was assessed on 1 % agarose gel electrophoresis. RNA concentration was measured using a NanoDrop 2000 spectrophotometer (Thermo Scientific). According to manufacturer instructions, 1 μg of RNA was used for reverse transcription using the iScript cDNA synthesis kit (BioRad, Madrid, Spain) on a MiniAmp Thermal Cycler (Thermo Scientific). After cDNA synthesis, reactions were performed using the SYBR Green Master Mix (Maxima SYBR Green qPCR Master Mix (K0252-ThermoScientific) on a LightCycler 480 PCR system (Roche Applied Science). *cdc-42* was used as the endogenous control gene, FW: CTGCTGGACAGGAAGATTACG; RV: CTCGGACATTCTCGAATGAAG. For *crt-1* expression the following primers were used, FW: GATGGGTTCAATCCAAGCACAAG; RV: CTCGGACATTCTCGAATGAAG. For $Aß_{1–42}$ expression the following primers were used, FW: GCAGAATTCCGACATGACTCAG; RV: GCCCACCATGAGTCCAATGA. The following program parameters were used for all amplifications: 95 °C for 10 min, followed by 45 cycles at 95 °C for 15 s, 60 °C for 30 s and 72 °C for 30 s, and finally one cycle at 95 °C for 20 min, 65 °C for 1 min, and 97 °C for 5 min. Assays were performed using three biological replicates, each with three technical replicates.

4.4. Paralysis assays

GMC101 and N2 worms maintained at 20 °C were developmentally synchronized by bleaching. 10–15 worms per experimental condition at young adult stage were transferred to new NGM agar plates containing HT115 *crt-1* RNAi, L4440 or HT115 *crt-1* RNAi / L4440 mixed bacteria at different percentages as a food source. Worms were shifted from 20 °C to 25 °C to induce the characteristic paralysis phenotype of the strain. 4 and 8 days after the temperature insult nematodes were scored for paralysis. Nematodes are scored as paralyzed if they fail to complete full body movement (*i.e.* a point of inflection traversing the entire body length) either spontaneously or touch-provoked, following the criteria previously described [39].

4.5. Free mobility assays

Tracking assays were performed at days 1, 3 and 5 of the adult stage. 10–20 young adult nematodes were placed in 35 mm NGM agar plates containing HT115 *crt-1* RNAi, L4440 or HT115 *crt-1* RNAi / L4440 mixed bacteria at different percentages as a food source, and next shifted from 20 °C to 25 °C. The plate was gently hit on the top of a flat surface to stimulate nematode movement. Immediately after, plates were placed under the stereomicroscope (Leica S9i), and an area containing around 5–10 worms was recorded for 30 s. Videos were analyzed with the Fiji plugin "wrMTrck", to obtain length traveled, body lengths per second (BLPS), average and maximum speed.

4.6. Measurements of mitochondrial membrane potential and mitochondrial ROS production

Mitochondrial membrane potential was measured on day 4 of adulthood in N2 and GMC101 worms. For each experimental condition, 10–20 worms were collected in 250 μl of M9 buffer using an eyelash to avoid bacterial contamination. For mitochondrial membrane potential measurements, nematodes were incubated for 3.5 h in 500 μl of M9 buffer containing 0.1 μM TMRE under shaking conditions, followed by

washing with M9 buffer. For mitochondrial ROS production measurements, nematodes were incubated for 4.5 h in 500 µl of M9 buffer containing 2 µM MitoSOX™ under shaking conditions. Worms were then washed with M9, placed on an empty plate and carefully transferred to 2 % agarose pads containing a drop of 50 mM tetramisole for immobilization. TMRM images were obtained using a Nikon ECLIPSE Ni-E fluorescence microscope equipped with a TRITC filter (excitation 540/25, emission 605/55) and a DS-Ri2 camera, or a Leica TCS SP5 confocal microscope (excitation 549 nm, emission 574 nm). MitoSOX™ images were obtained using a Nikon ECLIPSE Ni-E fluorescence microscope equipped with a TRITC filter. Each biological replicate was normalized to the mean fluorescence intensity of the N2 strain. This procedure was repeated at least three times for every experimental condition.

4.7. Measurements of oxygen consumption rates

Oxygen consumption rates were measured as previously described (Koopman et al., 2016) using an XFe24 metabolic analyzer (Agilent, United States). Day 4 synchronized worms were collected in 1 ml M9 buffer using an eyelash and transferred to an empty plate to avoid bacterial contamination. Next, 10–15 worms were transferred per well into a tissue culture plate (Seahorse, Agilent) containing 500 µl M9 buffer. Respiration rates were measured every 5 min using the following measurement protocol: 2 min mixing, 30 s waiting, and 2 min measuring. All experiments were performed at 25 °C. Respiratory chain modulators were added when indicated in the figures at the following concentrations: 10 µM FCCP; 50 mM Sodium Azide. Each well was normalized per number of worms using the Agilent Seahorse Analytics software. Then, recordings were exported to Prism and analyzed. Three biological replicates were performed per condition, each consisting in four technical replicates.

4.8. Measurements of the mitochondrial network in body-wall muscle cells

Muscle mitochondrial structure was measured as previously described in [40]. Day 4 synchronized worms were incubated for 24 h on NGM agar plates containing 5 µM TMRE added to the medium before pouring the plates. Thereafter, worms were washed with M9 and transferred for 30 min on regular NGM agar plates in the dark. Next, worms were carefully transferred to 2 % agarose pads containing a drop of 50 mM tetramisole for immobilization. Images were obtained on a Leica TCS SP5 confocal microscope (excitation: 549 nm, emission: 550–612 nm). Images were analyzed using the ImageJ plugin 'Mitochondria Analyzer' to quantify mitochondrial morphology parameters [62].

4.9. Measurements of ß-amyloid aggregates in vivo

Aß aggregates were measured *in vivo* using Thioflavin-T. Thioflavin-T was dissolved in M9 buffer and added just before pouring the plates to a final concentration of 50 µM. Day 4 synchronized worms were incubated for 24 h on NGM agar plates seeded with the appropriate RNAi-producing bacterial strain for each condition. Following incubation, nematodes were washed three times with M9 buffer and then incubated for 30 min on regular NGM agar plates in the dark. Worms were then carefully transferred to 2 % agarose pads containing a drop of 50 mM tetramisole. A coverslip was placed on top, and worms were imaged using a Leica TCS SP5 confocal microscope. Samples were excited with an argon laser at 458 nm and emission was collected at 470-553 nm. *Z*-stacks of 0.3–0.5 µm were acquired to capture the entire height of the worms. Images were analyzed using ImageJ software. *Z*-stack images were projected using the Image J tool 'Z-projection' to generate images including the full population of aggregates. A threshold was applied to ensure that all visible aggregates were captured, and regions of interest (ROIs) were manually checked to ensure all visible aggregates were included. ROI parameters including area, number, and fluorescence intensity were automatically measured with the Analyze Particle tool. N2 worms were used as a negative control to guarantee the specificity of the staining.

4.10. Western-blotting

400–500 worms on day 3 of adulthood were collected and washed three times. Pelleted worms were resuspended in 100 µl of RIPA buffer supplemented with protease inhibitors (Roche Applied Science, Spain) and phosSTOP phosphatase inhibitor cocktail (Roche, Spain), and subjected to three cycles of sonication (Vibra-Cell 75,115, Bioblock Scientific) at 4 °C. Each cycle was programmed as 10 s ON / 10 s OFF three times, with an amplitude of 39). After sonication, the lysate was centrifuged at 14,000 ×*g* for 20 min at 4 °C, and the protein content of the supernatant was determined using the Pierce® BCA Protein Assay Kit (ThermoFisher, Spain). An amount of 22 µg of total protein was loaded on SDS-PAGE gels (Bio-Rad). For immunoblotting, proteins were transferred onto nitrocellulose membrane with i-blot (Bio-Rad, Spain) and probed with the following antibodies: anti-actin (A3854, Merck) used at 1:200000 dilution, anti-beta amyloid peptide (6E10, BioLegend) used at 1:3000 dilution. Horseradish peroxidase–conjugated secondary antibodies were used at 1/10000 dilution (P0447, DakoCytomation), followed by chemiluminescence detection (SuperSignal™ West Pic PLUS Chemiluminescent Substrate, Thermo Scientific).

4.11. Statistical analysis

Statistical analyses were performed using Prism software (GraphPad). All data sets were tested for normal distribution using the Kolmogorov-Smirnov test. Unless otherwise indicated, significance between two experimental groups was determined using a two-tailed unpaired Student's *t*-test whereas group sets were analyzed using a one-way ANOVA (post-hoc Tukey test). NS, not significant; $*P < 0.05$; $**P < 0.01$; $***P < 0.001$; $****P < 0.0001$.

Supplementary data to this article can be found online at https://doi.org/10.1016/j.bbadis.2025.167946.

Funding

This work was supported by a grant from the Spanish Ministerio de Ciencia e Innovación [Ref. PID2021-122239OB-I00, co-financed by the European Union through the European Regional Development Fund]; Junta de Castilla y Leon (Spain) [Ref. CL-EI-2021]; the University of Valladolid [POSTDOC SEN-2019 UVA27]. S.R.-S. and E.C.-E. have a fellowship from the University of Valladolid. P.G.-C. has a Margarita Salas contract.

Declaration of competing interest

The authors declare the following financial interests/personal relationships which may be considered as potential competing interests: Jaime Santo-Domingo reports financial support was provided by University of Valladolid (Spain). Javier Alvarez reports financial support was provided by Agencia Estatal de Investigación (Spain). Jaime Santo-Domingo was previously employed by Nestle Research (Switzerland). If there are other authors, they declare that they have no known competing financial interests or personal relationships that could have appeared to influence the work reported in this paper.

Acknowledgements

The authors thank Jorge Mondejar-Duran for kindly providing the actin and beta-amyloid antibodies; Diego Sanchez and Maria Dolores Ganfornina for technical advice on RNA isolation procedures; Silvia Fernandez Martinez at the IBGM Metabolic and Cellular Analysis Unit,

for technical support with Seahorse experiments; Cristina Sanchez at the IBGM Microscopy Unit, for technical support on confocal microscopy experiments.

Data availability

The raw data supporting the conclusions of this manuscript will be made available by the authors, without undue reservation, to any qualified researcher.

References

[1] D.S. Knopman, H. Amieva, R.C. Petersen, G. Chételat, D.M. Holtzman, B.T. Hyman, R.A. Nixon, D.T. Jones, Alzheimer disease, Nat. Rev. Dis. Primers 7 (2021) 1–21, https://doi.org/10.1038/s41572-021-00269-y.

[2] K.Y. Chan, W. Wang, J.J. Wu, L. Liu, E. Theodoratou, J. Car, L. Middleton, T. C. Russ, I.J. Deary, H. Campbell, W. Wang, I. Rudan, Epidemiology of Alzheimer's disease and other forms of dementia in China, 1990–2010: a systematic review and analysis, Lancet 381 (2013) 2016–2023, https://doi.org/10.1016/S0140-6736(13)60221-4.

[3] A.A. Tahami Monfared, M.J. Byrnes, L.A. White, Q. Zhang, Alzheimer's disease: epidemiology and clinical progression, Neurol. Ther. 11 (2022) 553–569, https://doi.org/10.1007/s40120-022-00338-8.

[4] J. Zhang, Y. Zhang, J. Wang, Y. Xia, J. Zhang, L. Chen, Recent advances in Alzheimer's disease: mechanisms, clinical trials and new drug development strategies, Signal Transduct. Target. Ther. 9 (2024) 1–35, https://doi.org/10.1038/s41392-024-01911-3.

[5] J.M. Long, D.M. Holtzman, Alzheimer disease: an update on pathobiology and treatment strategies, Cell 179 (2019) 312–339, https://doi.org/10.1016/j.cell.2019.09.001.

[6] B. Dunn, P. Stein, P. Cavazzoni, Approval of Aducanumab for Alzheimer disease-the FDA'S perspective, JAMA Intern. Med. 181 (2021) 1276–1278, https://doi.org/10.1001/jamainternmed.2021.4607.

[7] J. Sevigny, P. Chiao, T. Bussière, P.H. Weinreb, L. Williams, M. Maier, R. Dunstan, S. Salloway, T. Chen, Y. Ling, J. O'Gorman, F. Qian, M. Arastu, M. Li, S. Chollate, M.S. Brennan, O. Quintero-Monzon, R.H. Scannevin, H.M. Arnold, T. Engber, K. Rhodes, J. Ferrero, Y. Hang, A. Mikulskis, J. Grimm, C. Hock, R.M. Nitsch, A. Sandrock, The antibody aducanumab reduces aβ plaques in Alzheimer's disease, Nature 537 (2016) 50–56, https://doi.org/10.1038/nature19323.

[8] J.D. Buxbaum, A.A. Ruefli, C.A. Parker, A.M. Cypess, P. Greengard, Calcium regulates processing of the Alzheimer amyloid protein precursor in a protein kinase C-independent manner, Proc. Natl. Acad. Sci. USA 91 (1994) 4489–4493, https://doi.org/10.1073/pnas.91.10.4489.

[9] M.P. Mattson, Antigenic changes similar to those seen in neurofibrillary tangles are elicited by glutamate and Ca2+ influx in cultured hippocampal neurons, Neuron 4 (1990) 105–117, https://doi.org/10.1016/0896-6273(90)90447-n.

[10] H.W. Querfurth, D.J. Selkoe, Calcium ionophore increases amyloid beta peptide production by cultured cells, Biochemistry 33 (1994) 4550–4561, https://doi.org/10.1021/bi00181a016.

[11] F.M. LaFerla, Calcium dyshomeostasis and intracellular signalling in Alzheimer's disease, Nat. Rev. Neurosci. 3 (2002) 862–872, https://doi.org/10.1038/nrn960.

[12] M. Kawahara, Y. Kuroda, Molecular mechanism of neurodegeneration induced by Alzheimer's beta-amyloid protein: channel formation and disruption of calcium homeostasis, Brain Res. Bull. 53 (2000) 389–397, https://doi.org/10.1016/s0361-9230(00)00370-1.

[13] K.N. Green, A. Demuro, Y. Akbari, B.D. Hitt, I.F. Smith, I. Parker, F.M. LaFerla, SERCA pump activity is physiologically regulated by presenilin and regulates amyloid beta production, J. Cell Biol. 181 (2008) 1107–1116, https://doi.org/10.1083/jcb.200706171.

[14] G.E. Stutzmann, I. Smith, A. Caccamo, S. Oddo, I. Parker, F. Laferla, Enhanced ryanodine-mediated calcium release in mutant PS1-expressing Alzheimer's mouse models, Ann. N. Y. Acad. Sci. 1097 (2007) 265–277, https://doi.org/10.1196/annals.1379.025.

[15] H. Tu, O. Nelson, A. Bezprozvanny, Z. Wang, S.-F. Lee, Y.-H. Hao, L. Serneels, B. De Strooper, G. Yu, I. Bezprozvanny, Presenilins form ER Ca2+ leak channels, a function disrupted by familial Alzheimer's disease-linked mutations, Cell 126 (2006) 981–993, https://doi.org/10.1016/j.cell.2006.06.059.

[16] J.G. Begley, W. Duan, S. Chan, K. Duff, M.P. Mattson, Altered calcium homeostasis and mitochondrial dysfunction in cortical synaptic compartments of presenilin-1 mutant mice, J. Neurochem. 72 (1999) 1030–1039, https://doi.org/10.1046/j.1471-4159.1999.0721030.x.

[17] M.A. Leissring, B.A. Paul, I. Parker, C.W. Cotman, F.M. LaFerla, Alzheimer's presenilin-1 mutation potentiates inositol 1,4,5-trisphosphate-mediated calcium signaling in Xenopus oocytes, J. Neurochem. 72 (1999) 1061–1068, https://doi.org/10.1046/j.1471-4159.1999.0721061.x.

[18] K. Princen, T. Van Dooren, M. van Gorsel, N. Louros, X. Yang, M. Dumbacher, I. Bastiaens, K. Coupet, S. Dupont, E. Cuveliers, A. Lauwers, M. Laghmouchi, T. Vanwelden, S. Carmans, N. Van Damme, H. Duhamel, S. Vansteenkiste, J. Prerad, K. Pipeleers, O. Rodiers, L. De Ridder, S. Claes, Y. Busschots, L. Pringels, V. Verhelst, E. Debroux, M. Brouwer, S. Lievens, J. Tavernier, M. Farinelli, S. Hughes-Asceri, M. Voets, J. Winderickx, S. Wera, J. de Wit, J. Schymkowitz, F. Rousseau, H. Zetterberg, J.L. Cummings, W. Annaert, T. Cornelissen, H. De Winter, K. De Witte, M. Fivaz, G. Griffioen, Pharmacological modulation of septins restores calcium homeostasis and is neuroprotective in models of Alzheimer's disease, Science 384 (2024) eadd6260, https://doi.org/10.1126/science.add6260.

[19] B.J. Park, D.G. Lee, J.R. Yu, S.K. Jung, K. Choi, J. Lee, J. Lee, Y.S. Kim, J.I. Lee, J. Y. Kwon, J. Lee, A. Singson, W.K. Song, S.H. Eom, C.S. Park, D.H. Kim, J. Bandyopadhyay, J. Ahnn, Calreticulin, a calcium-binding molecular chaperone, is required for stress response and fertility in Caenorhabditis elegans, Mol. Biol. Cell 12 (2001) 2835–2845, https://doi.org/10.1091/mbc.12.9.2835.

[20] R. Benyair, E. Ron, G.Z. Lederkremer, Chapter five - protein quality control, retention, and degradation at the endoplasmic reticulum, in: K.W. Jeon (Ed.), Int. Rev. Cell Mol. Biol., Academic Press, 2011, pp. 197–280, https://doi.org/10.1016/B978-0-12-386033-0.00005-0.

[21] M. Michalak, Calreticulin: Endoplasmic reticulum Ca2+ gatekeeper, J. Cell. Mol. Med. 28 (2024) e17839, https://doi.org/10.1111/jcmm.17839.

[22] Z. Sun, J.L. Brodsky, Protein quality control in the secretory pathway, J. Cell Biol. 218 (2019) 3171–3187, https://doi.org/10.1083/jcb.201906047.

[23] S. Baksh, M. Michalak, Expression of calreticulin in Escherichia coli and identification of its Ca2+ binding domains, J. Biol. Chem. 266 (1991) 21458–21465.

[24] P. Camacho, J.D. Lechleiter, Calreticulin inhibits repetitive intracellular Ca2+ waves, Cell 82 (1995) 765–771, https://doi.org/10.1016/0092-8674(95)90473-5.

[25] L.M. John, J.D. Lechleiter, P. Camacho, Differential modulation of SERCA2 isoforms by calreticulin, J. Cell Biol. 142 (1998) 963–973, https://doi.org/10.1083/jcb.142.4.963.

[26] L. Mery, N. Mesaeli, M. Michalak, M. Opas, D.P. Lew, K.H. Krause, Overexpression of calreticulin increases intracellular Ca2+ storage and decreases store-operated Ca2+ influx, J. Biol. Chem. 271 (1996) 9332–9339, https://doi.org/10.1074/jbc.271.16.9332.

[27] Q, L., Y, C., J, G. Serum calreticulin is a negative biomarker in patients with Alzheimer's disease. PubMed (2014). https://pubmed.ncbi.nlm.nih.gov/25429433/ (accessed May 12, 2025).

[28] T., J, F., A, F., Y, T., Y, T., M, T., Y, W., I, Y., T. Different expression of calreticulin and immunoglobulin binding protein in Alzheimer's disease brain. PubMed (n.d.). https://pubmed.ncbi.nlm.nih.gov/10963362/ (accessed May 12, 2025).

[29] Km, R., Eja, K., Ca, B., Toj, C., Gc, B. Brain cells release calreticulin that attracts and activates microglia, and inhibits amyloid beta aggregation and neurotoxicity. PubMed, 2022. https://pubmed.ncbi.nlm.nih.gov/35514983/ (accessed May 12, 2025).

[30] D. K, H. Pr, H. G, Interaction of calreticulin with amyloid beta peptide 1–42, PubMed (n.d.). https://pubmed.ncbi.nlm.nih.gov/18221019/ (accessed May 12, 2025).

[31] S. N, S. E, D. N, P. F, L. G, L. D, B. F, M. M, S. M, K. R, Generation of amyloid-β is reduced by the interaction of calreticulin with amyloid precursor protein, presenilin and nicastrin, PubMed (2013). https://pubmed.ncbi.nlm.nih.gov/23585889/ (accessed May 12, 2025).

[32] X, L., Ga, W., J, Z., He, G., T, I. C1q-calreticulin induced oxidative neurotoxicity: relevance for the neuropathogenesis of Alzheimer's disease. PubMed (n.d.). https://pubmed.ncbi.nlm.nih.gov/12576225/ (accessed May 12, 2025).

[33] J. Alvarez, P. Alvarez-Illera, P. García-Casas, R.I. Fonteriz, M. Montero, The role of Ca2+ signaling in aging and neurodegeneration: insights from Caenorhabditis elegans models, Cells 9 (2020) 204, https://doi.org/10.3390/cells9010204.

[34] B. Barbagallo, H.A. Prescott, P. Boyle, J. Climer, M.M. Francis, A dominant mutation in a neuronal acetylcholine receptor subunit leads to motor neuron degeneration in Caenorhabditis elegans, J. Neurosci. 30 (2010) 13932–13942, https://doi.org/10.1523/JNEUROSCI.1515-10.2010.

[35] A. Nagarajan, Y. Ning, K. Reisner, Z. Buraei, J.P. Larsen, O. Hobert, M. Doitsidou, Progressive degeneration of dopaminergic neurons through TRP channel-induced cell death, J. Neurosci. 34 (2014) 5738–5746, https://doi.org/10.1523/JNEUROSCI.4540-13.2014.

[36] J.E. Tanis, Z. Ma, P. Krajacic, L. He, J.K. Foskett, T. Lamitina, CLHM-1 is a functionally conserved and conditionally toxic Ca2+−permeable ion channel in Caenorhabditis elegans, J. Neurosci. 33 (2013) 12275–12286, https://doi.org/10.1523/JNEUROSCI.5919-12.2013.

[37] L.R. Earls, M.L. Hacker, J.D. Watson, D.M. Miller, Coenzyme Q protects Caenorhabditis elegans GABA neurons from calcium-dependent degeneration, Proc. Natl. Acad. Sci. USA 107 (2010) 14460–14465, https://doi.org/10.1073/pnas.0910630107.

[38] L.E.A. Young, C. Shoben, K. Ricci, D.C. Williams, Genetic analysis of KillerRed in C. Elegans identifies a shared role of calcium genes in ROS-mediated neurodegeneration, J. Neurogenet. 33 (2019) 1–9, https://doi.org/10.1080/01677063.2018.1531857.

[39] G. McColl, B.R. Roberts, T.L. Pukala, V.B. Kenche, C.M. Roberts, C.D. Link, T. M. Ryan, C.L. Masters, K.J. Barnham, A.I. Bush, R.A. Cherny, Utility of an improved model of amyloid-beta ($aβ_{1-42}$) toxicity in Caenorhabditis elegans for drug screening for Alzheimer's disease, Mol. Neurodegener. 7 (2012) 57, https://doi.org/10.1186/1750-1326-7-57.

[40] M. Romani, V. Sorrentino, C.-M. Oh, H. Li, T.I. de Lima, H. Zhang, M. Shong, J. Auwerx, NAD+ boosting reduces age-associated amyloidosis and restores mitochondrial homeostasis in muscle, Cell Rep. 34 (2021) 108660, https://doi.org/10.1016/j.celrep.2020.108660.

[41] L.F. Ng, J. Gruber, I.K. Cheah, C.K. Goo, W.F. Cheong, G. Shui, K.P. Sit, M.R. Wenk, B. Halliwell, The mitochondria-targeted antioxidant MitoQ extends lifespan and improves healthspan of a transgenic Caenorhabditis elegans model of Alzheimer disease, Free Radic. Biol. Med. 71 (2014) 390–401, https://doi.org/10.1016/j.freeradbiomed.2014.03.003.

[42] A. Andra, S. Tanigawa, T. Bito, A. Ishihara, F. Watanabe, Y. Yabuta, Effects of vitamin B12 deficiency on amyloid-β toxicity in Caenorhabditis elegans, Antioxidants 10 (2021) 962, https://doi.org/10.3390/antiox10060962.
[43] T. Etheridge, M. Rahman, C.J. Gaffney, D. Shaw, F. Shephard, J. Magudia, D. E. Solomon, T. Milne, J. Blawzdziewicz, D. Constantin-Teodosiu, P.L. Greenhaff, S. A. Vanapalli, N.J. Szewczyk, The integrin-adhesome is required to maintain muscle structure, mitochondrial ATP production, and movement forces in Caenorhabditis elegans, FASEB, J. Off. Publ. Fed. Am. Soc. Exp. Biol. 29 (2015) 1235–1246, https://doi.org/10.1096/fj.14-259119.
[44] L. Lannfelt, C. Möller, H. Basun, G. Osswald, D. Sehlin, A. Satlin, V. Logovinsky, P. Gellerfors, Perspectives on future Alzheimer therapies: amyloid-β protofibrils - a new target for immunotherapy with BAN2401 in Alzheimer's disease, Alzheimers Res. Ther. 6 (2014) 16, https://doi.org/10.1186/alzrt246.
[45] V. Sorrentino, M. Romani, L. Mouchiroud, J.S. Beck, H. Zhang, D. D'Amico, N. Moullan, F. Potenza, A.W. Schmid, S. Rietsch, S.E. Counts, J. Auwerx, Enhancing mitochondrial proteostasis reduces amyloid-β proteotoxicity, Nature 552 (2017) 187–193, https://doi.org/10.1038/nature25143.
[46] P. García-Casas, P. Alvarez-Illera, R.I. Fonteriz, M. Montero, J. Alvarez, Mechanism of the lifespan extension induced by submaximal SERCA inhibition in C. Elegans, Mech. Ageing Dev. 196 (2021) 111474, https://doi.org/10.1016/j.mad.2021.111474.
[47] P. García-Casas, J. Arias-Del-Val, P. Alvarez-Illera, R.I. Fonteriz, M. Montero, J. Alvarez, Inhibition of Sarco-endoplasmic reticulum Ca2+ ATPase extends the lifespan in C. Elegans Worms, Front. Pharmacol. 9 (2018) 669, https://doi.org/10.3389/fphar.2018.00669.
[48] S. Romero-Sanz, E. Caldero-Escudero, P. Álvarez-Illera, J. Santo-Domingo, R. I. Fonteriz, M. Montero, J. Álvarez, SERCA inhibition improves lifespan and healthspan in a chemical model of Parkinson disease in Caenorhabditis elegans, Front. Pharmacol. 14 (2023) 1182428, https://doi.org/10.3389/fphar.2023.1182428.
[49] L.R. H, L. Dh, C. Ak, K. Jm, Role of calreticulin in regulating intracellular Ca2+ storage and capacitative Ca2+ entry in HeLa cells, PubMed (n.d.). https://pubmed.ncbi.nlm.nih.gov/9883279/ (accessed May 12, 2025).
[50] C.J. Gaffney, F. Shephard, J. Chu, D.L. Baillie, A. Rose, D. Constantin-Teodosiu, P. L. Greenhaff, N.J. Szewczyk, Degenerin channel activation causes caspase-mediated protein degradation and mitochondrial dysfunction in adult *C. elegans* muscle, J. Cachexia. Sarcopenia Muscle 7 (2015) 181, https://doi.org/10.1002/jcsm.12040.
[51] K. Xu, N. Tavernarakis, M. Driscoll, Necrotic cell death in C. Elegans requires the function of calreticulin and regulators of Ca(2+) release from the endoplasmic reticulum, Neuron 31 (2001) 957–971, https://doi.org/10.1016/s0896-6273(01)00432-9.
[52] W. Lee, K.R. Kim, G. Singaravelu, B.-J. Park, D.H. Kim, J. Ahnn, Y.J. Yoo, Alternative chaperone machinery may compensate for calreticulin/calnexin deficiency in Caenorhabditis elegans, Proteomics 6 (2006) 1329–1339, https://doi.org/10.1002/pmic.200500320.
[53] D. Lee, G. Singaravelu, B.-J. Park, J. Ahnn, Differential requirement of unfolded protein response pathway for Calreticulin expression in *Caenorhabditis elegans*, J. Mol. Biol. 372 (2007) 331–340, https://doi.org/10.1016/j.jmb.2007.06.071.
[54] C. Cheignon, M. Tomas, D. Bonnefont-Rousselot, P. Faller, C. Hureau, F. Collin, Oxidative stress and the amyloid beta peptide in Alzheimer's disease, Redox Biol. 14 (2018) 450–464, https://doi.org/10.1016/j.redox.2017.10.014.
[55] F. Muñoz-Lobato, M.J. Rodríguez-Palero, F.J. Naranjo-Galindo, F. Shephard, C. J. Gaffney, N.J. Szewczyk, S. Hamamichi, K.A. Caldwell, G.A. Caldwell, C.D. Link, A. Miranda-Vizuete, Protective role of DNJ-27/ERdj5 in Caenorhabditis elegans models of human neurodegenerative diseases, Antioxid. Redox Signal. 20 (2014) 217–235, https://doi.org/10.1089/ars.2012.5051.
[56] A. Ciechanover, Y.T. Kwon, Degradation of misfolded proteins in neurodegenerative diseases: therapeutic targets and strategies, Exp. Mol. Med. 47 (2015) e147, https://doi.org/10.1038/emm.2014.117.
[57] V. Kapulkin, B.G. Hiester, C.D. Link, Compensatory regulation among ER chaperones in C. Elegans, FEBS Lett. 579 (2005) 3063–3068, https://doi.org/10.1016/j.febslet.2005.04.062.
[58] L., S, F., S, La, J, Nj, S. Integrated control of protein degradation in *C. elegans* muscle. PubMed (2012). https://pubmed.ncbi.nlm.nih.gov/23457662/ (accessed May 12, 2025).
[59] Ml, F.-M., La, H., G, F., Mt, B., Cd, L. Decreased insulin-receptor signaling promotes the autophagic degradation of beta-amyloid peptide in *C. elegans*, PubMed (n.d.). https://pubmed.ncbi.nlm.nih.gov/17675890/ (accessed May 12, 2025).
[60] B. Md, C. T, B. G, P. Jb, R. K, The regulation of autophagy by calcium signals: Do we have a consensus?, PubMed (n.d.). https://pubmed.ncbi.nlm.nih.gov/28847414/ (accessed May 12, 2025).
[61] E. Panagiotidou, A. Gioran, D. Bano, N. Chondrogianni, Neuron-specific proteasome activation exerts cell non-autonomous protection against amyloid-beta (aβ) proteotoxicity in Caenorhabditis elegans, Redox Biol. 65 (2023) 102817, https://doi.org/10.1016/j.redox.2023.102817.
[62] A. Chaudhry, R. Shi, D.S. Luciani, A pipeline for multidimensional confocal analysis of mitochondrial morphology, function, and dynamics in pancreatic β-cells, Am. J. Physiol. Endocrinol. Metab. 318 (2020) E87–E101, https://doi.org/10.1152/ajpendo.00457.2019.